JOURNAL OF GUIDANCE, CONTROL, AND DYNAMICS
Vol. 35, No. 1, January–February 2012

Engineering Notes

Relative State Estimation and Observability Analysis for Formation Flying Satellites

Daan Maessen* and Eberhard Gill†
Delft University of Technology, 2629 HS Delft, The Netherlands

DOI: 10.2514/1.55125

I. Introduction

TO AUTONOMOUSLY control a satellite formation, the relative position and velocity of the satellites needs to be estimated. For tight formations, all the required information needs to be obtained and processed onboard the satellites. In case absolute position measurements, such as provided by the Global Positioning System (GPS), cannot be obtained, estimation of the absolute or relative state requires the satellites to autonomously measure the intersatellite range and/or line-of-sight angles. Markley [1], Herklotz [2], Psiaki [3], Liu and Liu [4], and Yim et al. [5] have analyzed the problem of autonomous absolute orbit determination using intersatellite vector measurements whereas Markley [1], Woffinden and Geller [6–8], Chen and Xu [9], Doolittle et al. [10], Chavez and Lovell [11], Holt and Lightsey [12], Kang et al. [13], and Matko et al. [14] studied the problem of autonomous relative orbit determination using intersatellite measurements. Several authors furthermore studied the effect of intersatellite ranging to augment external measurements like those from GPS and ground stations for either absolute or relative orbit determination. Amongst these are Holt and Lightsey [15], Huxel [16], and Huxel and Bishop [17,18].

Although previous work has been quite extensive, the understanding of the results obtained in some of these works needs to be improved by performing a detailed study of the observability of the system as a function of the relative state and of sensor suite properties, such as sensor accuracy and sensor placement. In addition, as no reference has been found in the literature, a further objective of this research is to provide a derivation of the expected value and variance, in three dimensions, in the estimation of the relative position of two objects.

To isolate the basic properties of interest, a simple setting is implemented. The rationale behind this is that more advanced and realistic effects add only minor contributions and effects to the findings while they add considerable complexity to the analysis of the results. Two satellites, a chief and a deputy, are flying in formation in a low-Earth orbit (LEO) and perform intersatellite range measurements using locally generated one-way radio frequency ranging signals. The chief uses either one or three receiver (Rx) antennas to acquire and track the ranging signal transmitted by the deputy and to determine the relative range(s). The range measurements are treated together with a linearized dynamic model of the satellites' relative motion to estimate their relative orbit using an iterative batch least-squares (LSQ) algorithm. An observability analysis is performed to gain a deeper insight in the obtained results.

Received 31 May 2011; revision received 4 August 2011; accepted for publication 8 August 2011.

*Ph.D. Candidate, Department of Space Engineering, Kluyverweg 1, Delft; d.c.maessen@tudelft.nl. Student Member AIAA (Corresponding Author).

†Professor of Space Systems Engineering, Department of Space Engineering, Kluyverweg 1, Delft.

II. Orbital Dynamics Modeling

The relative motion of the satellites is described in the Hill frame [19], which is centered at the chief and has unit vectors, $\boldsymbol{e}_x$, $\boldsymbol{e}_y$, and $\boldsymbol{e}_z$, with $\boldsymbol{e}_x$ pointing radially outward, $\boldsymbol{e}_z$ normal to the orbit and aligned with the orbit angular momentum vector, and $\boldsymbol{e}_y$ parallel to the velocity vector. The relative motion of the satellites is expressed through the state vector $\boldsymbol{x} \in \mathbb{R}^6$ and its associated set of rectilinear coordinates as $\boldsymbol{x} = (\boldsymbol{r}^T \quad \boldsymbol{v}^T)^T = (x \quad y \quad z \quad \dot{x} \quad \dot{y} \quad \dot{z})^T$, where the vectors $\boldsymbol{r}$ and $\boldsymbol{v}$ contain the states that denote the relative positions, $(x \quad y \quad z)^T$, and velocities, $(\dot{x} \quad \dot{y} \quad \dot{z})^T$, respectively. The body reference frame of the chief is aligned with the Hill frame.

In state-space form, the Clohessy-Wiltshire (CW) equations express the linearized relative motion dynamics in the Hill frame [20] as

$$\dot{\boldsymbol{x}}(t) = \boldsymbol{A}\boldsymbol{x}(t) = \begin{pmatrix} 0 & 0 & 0 & 1 & 0 & 0 \\ 0 & 0 & 0 & 0 & 1 & 0 \\ 0 & 0 & 0 & 0 & 0 & 1 \\ 3n^2 & 0 & 0 & 0 & 2n & 0 \\ 0 & 0 & 0 & -2n & 0 & 0 \\ 0 & 0 & -n^2 & 0 & 0 & 0 \end{pmatrix} \boldsymbol{x}(t) \tag{1}$$

where $\boldsymbol{A}$ is the system matrix, t denotes time, and n denotes the orbital mean motion of the chief. The homogeneous solution to Eq. (1) is $\boldsymbol{x}(t) = \boldsymbol{\Phi}(t, 0)\boldsymbol{x}(0)$ with the state transition matrix, $\boldsymbol{\Phi}(t, 0)$, mapping the state at time $t_0 = 0$ to the state at time t. The elements of $\boldsymbol{\Phi}(t, 0)$ are provided by multiple references, such as Alfriend et al. [20].

III. Statistical Analysis of the Relative Position Estimation Problem

In this section, a statistical treatment is used to derive expressions for the position estimate of a transmitter (Tx) antenna with respect to a reference frame defined by three receiver antennas, Rx_0, Rx_1, and Rx_2, as shown in Fig. 1a. The distances between Rx_0 and Rx_1 and between Rx_0 and Rx_2 are equal to d_1 and d_2, respectively. The Tx antenna is located at coordinates, $(x_{\mathrm{Tx}}, y_{\mathrm{Tx}}, z_{\mathrm{Tx}})$; the true range between antennas Rx_i and Tx is r_i; the measured pseudorange is ρ_i; and the ranging accuracy is σ_{ρ_i} with $i = 0, 1, 2$.

Because d_1, d_2, r_0, r_1, and r_2 are known, two triangles with known side lengths, Rx_0-Rx_1-Tx and Rx_0-Rx_2-Tx, can be formed, as seen in Fig. 1b. The following three equations can be constructed for the angles defined in Fig. 1b:

$$\cos\beta_0 = \frac{r_0^2 - r_1^2 + d_1^2}{2r_0 d_1} = \frac{\boldsymbol{r}_0 \bullet \boldsymbol{d}_1}{\|\boldsymbol{r}_0\|\|\boldsymbol{d}_1\|} \tag{2a}$$

$$\cos\gamma_0 = \frac{r_0^2 - r_2^2 + d_2^2}{2r_0 d_2} = \frac{\boldsymbol{r}_0 \bullet \boldsymbol{d}_2}{\|\boldsymbol{r}_0\|\|\boldsymbol{d}_2\|} \tag{2b}$$

$$\cos\beta = \frac{r_0^2 + r_1^2 - d_1^2}{2r_0 r_1} = \frac{\boldsymbol{r}_0 \bullet \boldsymbol{r}_1}{\|\boldsymbol{r}_0\|\|\boldsymbol{r}_1\|} \tag{2c}$$

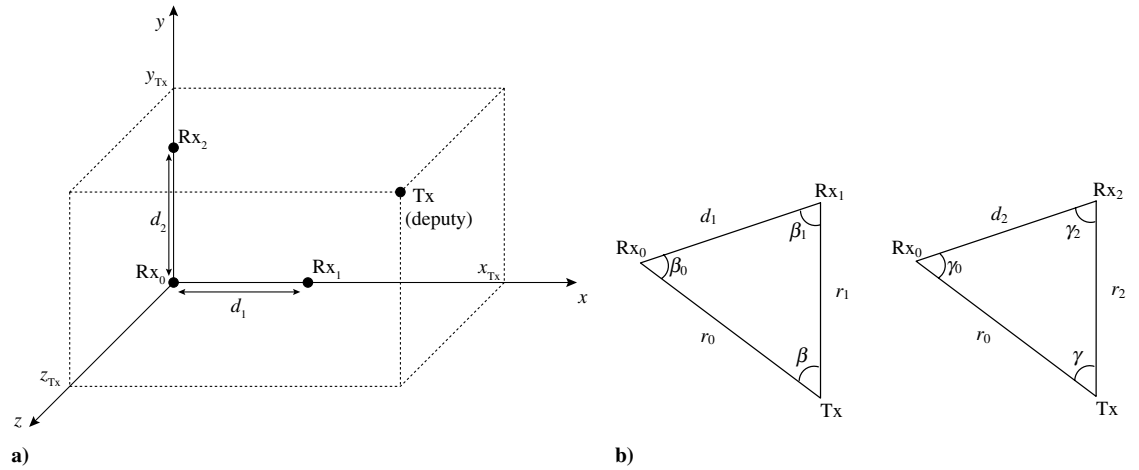

Fig. 1 a) Location of the various antennas in the receiver reference frame and b) definition of the angles in the triangles formed by the Tx and Rx antennas.

with $\|\cdot\|$ denoting the Euclidian vector norm and $\boldsymbol{d}$ and $\boldsymbol{r}$ the vectors of the corresponding distances. Equations (2a–2c) are used to derive the following expressions for x_{Tx}, y_{Tx}, and z_{Tx}

$$x_{\mathrm{Tx}} = \frac{r_0^2 - r_1^2 + d_1^2}{2d_1} \tag{3a}$$

$$y_{\mathrm{Tx}} = \frac{r_0^2 - r_2^2 + d_2^2}{2d_2} \tag{3b}$$

$$z_{\mathrm{Tx}} = \frac{1}{2}\left(-\left(\frac{r_0^4}{d_1^2} + \frac{r_1^4}{d_1^2} - \frac{2r_0^2 r_1^2}{d_1^2} - 2r_1^2 + d_1^2\right) - \left(\frac{r_0^4}{d_2^2} + \frac{r_2^4}{d_2^2} - \frac{2r_0^2 r_2^2}{d_2^2} - 2r_2^2 + d_2^2\right)\right)^{1/2} \tag{3c}$$

By replacing the true range, r_i, with the pseudorange, $\rho_i \sim \mathcal{N}(r_i, \sigma_{\rho_i}^2)$, in Eqs. (3a–3c), expressions for the expected value and variance of the relative position estimate can be derived using a second-order multivariate Taylor expansion around r_i. In the derivation, zero cross-correlation between measurements from different Rx antennas is assumed. In addition, it is assumed that $\sigma_{\rho_i} = \sigma_\rho$. This leads to

$$x_{\mathrm{Tx}}|_{\sigma_\rho \ll r,d} \sim \mathcal{N}\left(\frac{r_0^2 - r_1^2 + d_1^2}{2d_1}, (r_0^2 + r_1^2)\frac{\sigma_\rho^2}{d_1^2}\right) \tag{4a}$$

$$y_{\mathrm{Tx}}|_{\sigma_\rho \ll r,d} \sim \mathcal{N}\left(\frac{r_0^2 - r_2^2 + d_2^2}{2d_2}, (r_0^2 + r_1^2)\frac{\sigma_\rho^2}{d_2^2}\right) \tag{4b}$$

$$z_{\mathrm{Tx}}|_{r_i = r, d_i = d, r \gg d, \sigma_\rho} \sim \mathcal{N}\left(r\left(1 - 2\frac{\sigma_\rho^2}{d^2}\right), 5r^2\frac{\sigma_\rho^4}{d^4}\right) \tag{4c}$$

Comparing Eqs. (4a–4c) with Eqs. (3a–3c) shows that for $\sigma_\rho/d \ll 1$ and $\sigma_\rho/r \ll 1$, the mean of the position estimate will be very close to the truth. These are reasonable conditions because r is commonly at least tens of meters, d is at least several decimeters, and σ_ρ is typically on the order of centimeters [21].

Equations (4a) and (4b) show that the standard deviation in the estimate of x_{Tx} and y_{Tx} depends linearly on r and σ_ρ and inversely linear on d. The standard deviation in the estimate of z_{Tx}, however, [cf. Equation (4c)] depends linearly on r but quadratically on σ_ρ and inversely quadratic on d. Thus, the estimate for z_{Tx} will usually be much more accurate than the estimates for x_{Tx} and y_{Tx} because it scales with $(\sigma_\rho/d)^2$ instead of σ_ρ/d and because $\sigma_\rho/d \ll 1$.

IV. Estimator Description and Observability Analysis

A. Batch Least-Squares Estimator

The pseudorange measurements ρ_i at time t are modeled as

$$\rho_i(t) = \|\mathbf{r}_i(t)\| + \varepsilon \tag{5}$$

with $\mathbf{r}_i(t) = (\,x(t) - x_{\mathrm{Rx}_i},\quad y(t) - y_{\mathrm{Rx}_i},\quad z(t) - z_{\mathrm{Rx}_i}\,)^T$ and ε as a normally distributed measurement noise. The system model is described in state-space notation as

$$\dot{\boldsymbol{x}}(t) = \boldsymbol{A}\boldsymbol{x}(t) \tag{6a}$$

$$\boldsymbol{z}\,(t) = \boldsymbol{h}(\boldsymbol{x}, t) + \boldsymbol{\epsilon} \tag{6b}$$

where the vector $\boldsymbol{z}(t)$ contains the pseudorange measurements ρ_i and where the expected measurements are modeled as a nonlinear function $\boldsymbol{h}(\boldsymbol{x}, t)$ of the system states as in Eq. (5). In Eq. (6a), it is implicitly assumed that the relative dynamics model perfectly describes the true dynamics, hence the absence of a process noise term. The statistics for the measurement noise, contained in the vector $\boldsymbol{\epsilon}$ are $E[\boldsymbol{\epsilon}] = \mathbf{0}$ and $E[\boldsymbol{\epsilon}\boldsymbol{\epsilon}^T] = \boldsymbol{W}^{-1} = \sigma^2 \boldsymbol{I}_j$, with $\boldsymbol{I}_j$ being the identity matrix of size $j \times j$, j being the number of Rx antennas ($j = \{1, 3\}$), and $\boldsymbol{W}$ a weighting matrix. Because $\boldsymbol{W}$ is diagonal, zero cross-correlation is implicitly assumed between measurements taken with different Rx antennas at the same epoch.

An iterative batch LSQ algorithm is used to find an estimate for the relative state at time $t_0 = 0$, which requires a linearization of Eq. (6b) around a reference state, $\boldsymbol{x}^{\mathrm{ref}}$. The estimator is given as

$$\hat{\boldsymbol{x}}_0^{\,k+1} = \hat{\boldsymbol{x}}_0^k + \boldsymbol{P}^k(\boldsymbol{\Lambda}(\boldsymbol{x}_0^{\mathrm{apr}} - \hat{\boldsymbol{x}}_0^k) + \tilde{\boldsymbol{H}}^{kT}\boldsymbol{W}\Delta\boldsymbol{z}^k) \tag{7}$$

where k denotes the number of iterations, $\boldsymbol{P}$ is the covariance matrix, $\boldsymbol{\Lambda}$ is a diagonal a priori information matrix, $\boldsymbol{x}_0^{\mathrm{apr}}$ is an a priori relative state estimate, $\tilde{\boldsymbol{H}}(t)$ is the measurement sensitivity matrix, and $\Delta\boldsymbol{z}(t) = \boldsymbol{z}(t) - \boldsymbol{h}(\hat{\boldsymbol{x}}^k, t)$. The covariance matrix, $\boldsymbol{P}$, is defined as

$$\boldsymbol{P}^k = (\boldsymbol{\Lambda} + \tilde{\boldsymbol{H}}^{kT}\boldsymbol{W}\tilde{\boldsymbol{H}}^k)^{-1} \tag{8}$$

and $\tilde{\boldsymbol{H}}(t)$ is defined as

$$\tilde{\boldsymbol{H}}^{\,k}(t) = \begin{pmatrix} \tilde{\boldsymbol{H}}_{t_0}^k \\ \tilde{\boldsymbol{H}}_{t_1}^k \\ \vdots \\ \tilde{\boldsymbol{H}}_{t_{m-1}}^k \end{pmatrix} = \begin{pmatrix} \boldsymbol{H}_{t_0}^k \boldsymbol{\Phi}(t_0, 0) \\ \boldsymbol{H}_{t_1}^k \boldsymbol{\Phi}(t_1, 0) \\ \vdots \\ \boldsymbol{H}_{t_{m-1}}^k \boldsymbol{\Phi}(t_{m-1}, 0) \end{pmatrix} \tag{9}$$

with $\boldsymbol{H} = \partial\boldsymbol{h}(\boldsymbol{x}, t)/\partial\boldsymbol{x}|_{\boldsymbol{x}=\boldsymbol{x}^{\mathrm{ref}}}$ and m as the total number of measurements.

B. Observability Analysis

The observability of the linear system can be determined by means of the observability Gramian, $\boldsymbol{G}$, which is defined for a discrete-time system [16] as

$$\boldsymbol{G} \triangleq \sum_{m=0}^{m-1} (\boldsymbol{H}(t_m)\boldsymbol{\Phi}(t_m,0))^T \boldsymbol{H}(t_m)\boldsymbol{\Phi}(t_m,0) = \tilde{\boldsymbol{H}}^T\tilde{\boldsymbol{H}} \tag{10}$$

If $\boldsymbol{G}$ is nonsingular, i.e., full rank, the system is observable for that particular state. Large eigenvalues for $\boldsymbol{G}$ result in good observability in the directions (eigenvectors) corresponding to those eigenvalues [22]. To allow a proper interpretation of its eigenvalues, $\boldsymbol{G}$ needs to be normalized [23]. Denoting the first three columns of $\tilde{\boldsymbol{H}}$ as $\tilde{\boldsymbol{H}}_r$ and the remaining three columns of $\tilde{\boldsymbol{H}}$ as $\tilde{\boldsymbol{H}}_v$, the following normalized Gramian, $\tilde{\boldsymbol{G}}$, is created:

$$\tilde{\boldsymbol{G}} = \boldsymbol{\Xi}^T\boldsymbol{\Xi} = (\,\tilde{\boldsymbol{H}}_r \quad n\tilde{\boldsymbol{H}}_v\,)^T(\,\tilde{\boldsymbol{H}}_r \quad n\tilde{\boldsymbol{H}}_v\,) \tag{11}$$

The eigenvalues and eigenvectors of $\tilde{\boldsymbol{G}}$ can be found by performing a singular value decomposition (SVD) of $\boldsymbol{\Xi}$ such that

$$\boldsymbol{\Xi} = \boldsymbol{U}\boldsymbol{\Sigma}\boldsymbol{V}^T \tag{12}$$

In Eq. (12), $\boldsymbol{\Sigma} = \mathrm{diag}(\Sigma_1, \Sigma_2, \ldots, \Sigma_6)$ with singular values $\Sigma_1 > \Sigma_2 > \ldots > \Sigma_6$, and $\boldsymbol{U}$ and $\boldsymbol{V}$ are orthonormal matrices. The singular values in $\boldsymbol{\Sigma}$ are the nonnegative square roots of the eigenvalues λ_i of $\tilde{\boldsymbol{G}}$. The columns v_i of the matrix $\boldsymbol{V}$ are the eigenvectors of $\tilde{\boldsymbol{G}}$, and v_i corresponds to Σ_i. Eigenvector v_1 is the most observable direction of the system, and the largest value in that vector is the most observable state. Furthermore, a small value for the condition number, κ, defined as the ratio of the largest and smallest singular value of a matrix [24], indicates a good accuracy in the estimate (well-conditioned) whereas a large value for κ indicates poor accuracy (ill-conditioned). Because the matrix that will actually be inverted is $\boldsymbol{G}$ and not $\tilde{\boldsymbol{G}}$, κ needs to be determined for the non-normalized matrix $\tilde{\boldsymbol{H}}$. Performing the SVD for $\tilde{\boldsymbol{H}}$ as

$$\tilde{\boldsymbol{H}} = \tilde{\boldsymbol{U}}\,\tilde{\boldsymbol{\Sigma}}\,\tilde{\boldsymbol{V}}^T \tag{13}$$

κ is equal to

$$\kappa(\tilde{\boldsymbol{\Sigma}}) = \frac{\tilde{\Sigma}_1}{\tilde{\Sigma}_6} \tag{14}$$

It is noted that, as pointed out by one of the reviewers, a 3×3 matrix can be constructed from the unit vectors pointing from the Rx antennas to the Tx antenna in Fig. 1a. When the volume defined by these unit vectors is sufficiently large (i.e., the determinant of the 3×3 matrix is nonzero or nonsingular) an estimate of the relative position can be obtained. Thus, the volume of this 3×3 matrix can also serve as a measure of observability.

V. Simulations

This section describes the setup and results of numerous simulations that have been performed to investigate the influence of the Rx antenna baseline, ranging accuracy, intersatellite distance, and relative state on the accuracy in the relative state estimation and on the observability of the relative state of two formation flying satellites in LEO.

A. Setup

Two types of formations that exhibit bounded 1:1 commensurate motion (i.e., the orbital periods of the chief and deputy match) are considered: a safe ellipse and a pendulum, as seen in Figure 2. As reported in Doolittle et al. [10] and Maessen and Gill [25], the accuracy in the relative navigation estimation can depend on the amount of cross-track motion. Therefore, the maximum cross-track distance in both formation geometries studied, $z_{\max}$, is varied between 0 and r_e, the intersatellite distance at epoch. Naturally, the term "safe" ellipse does not hold for small $z_{\max}$. The initial conditions for the formations are summarized in Table 1. The chief is in a circular LEO orbit with a semimajor axis of 7028 km.

The Rx antenna baseline, ranging accuracy, and intersatellite distance are also varied in magnitude, as shown in Table 2. In case of three Rx antennas, the Rx antennas on the chief are positioned at the normalized coordinates, $(-1/2, 0, 1/2)$, $(0, 1/2, -1/2)$, and $(1/2, -1/2, 0)$. The selected chief side lengths lead to antenna baselines of $(150)^{1/2}$ cm, $(150)^{1/2}$ dm, and $(150)^{1/2}$ m. In case of a single Rx antenna, the chief is assumed to be a point mass. Each Rx antenna performs 100 range measurements per orbit, and state estimations are performed for measurement arc lengths of 0.1 up to five orbits.

To avoid numerical complications arising from nonlinear effects, the error in the a priori state, $\Delta\boldsymbol{x}_0^0$, is set equal to $\Delta\boldsymbol{x}_0^0 = 1 \cdot 10^{-3}(\,r_e, \quad r_e, \quad r_e, \quad nr_e, \quad nr_e, \quad nr_e\,)^T$, and both the reference trajectory and the estimated trajectory are propagated using the CW equations. The a priori standard deviations are set to $0.1r_e$ in relative position, in the following denoted as σ^{apr}, and $0.1nr_e$ in relative velocity.

B. Results

1. Estimator Results and their link with the Statistical Analysis

The accuracy in the estimation of the relative state for both formation geometries is provided in Table 3 for a measurement arc length of five orbits. Only the three-dimensional (3-D) root sum squared (RSS) standard deviation, σ_{RSS}, in the relative position estimation error is provided. This figure of merit is considered to provide sufficient information on the convergence of the total state estimate. Two notable differences between the elliptical formation and the pendulum formation are evident. First, the results for the safe ellipse do not depend on $z_{\max}$, but they do depend on $z_{\max}$ for the pendulum formation. This is explained in the next subsection. Second, in case of a single Rx antenna the relative state estimate for

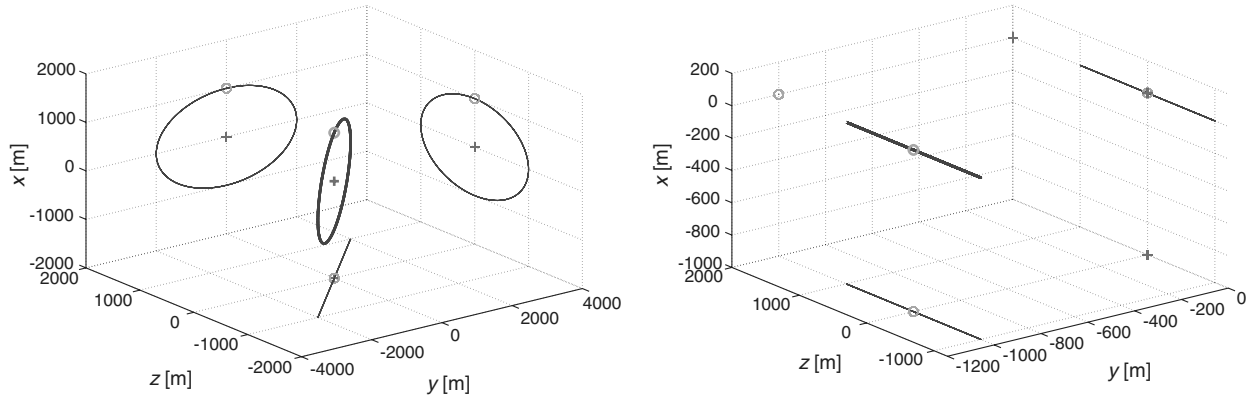

Fig. 2 a) Safe ellipse and b) pendulum trajectories in 3-D (bold) and their two-dimensional projections. The cross and the circle denote the positions of the chief and the deputy at t_0, respectively.

Table 1 Initial conditions for the formation geometries studied

Formation	x_0, m	y_0, m	z_0, m	$\dot{x}_0$, m/s	$\dot{y}_0$, m/s	$\dot{z}_0$, m/s
Safe ellipse	r_e	0	0	0	$-2nx_0$	$[-nx_0, 0]$
Pendulum	0	$-r_e$	0	0	0	$[0, ny_0]$

Table 2 Variations in simulation parameters

Parameter	Small	Medium	Large
Chief side length, m	0.1	1	10
Ranging accuracy σ_ρ, m	0.01	0.1	1
Intersatellite distance at t_0 (r_e), km	0.1	1	10

the pendulum formation can be improved well beyond σ^{apr}, whereas this is hardly the case for the safe ellipse.

Table 3 further shows that for both formation geometries and for small ratios of $z_{\max}/r_e$, an estimator divergence occurs, implying that the absolute error in the estimate of a state is larger than three times the standard deviation in the estimate of that state. This phenomenon is usually referred to in literature as "apparent" filter divergence [26], but because a batch estimator is used instead of a recursive filter, here it is referred to as estimator divergence. Its cause is further analyzed in the second part of this subsection.

The nonlinear empirical relationship in Table 3 for the safe ellipse and three Rx antennas is caused by the usage of the information matrix, $\mathbf{\Lambda}$, in the estimator, which leads to a convergence of σ_{RSS} to σ^{apr} for large σ_ρ/d (cf. Fig 3), implying that the measurements provide poor information for this condition. In fact, for large σ_ρ/d, the result is no longer better than what can be achieved using a single Rx antenna. Figure 3 also shows the linear approximation $\sigma_{\text{RSS}} = (r_e\sigma_\rho)/(9d)$, which provides a good fit for the simulation data for small σ_ρ/d and holds approximately up to $\sigma_\rho/d = 0.25$ for the current choice for the elements of $\mathbf{\Lambda}$. This approximation is in close agreement with the statistical result for σ_{RSS}, which, for a single measurement epoch, is equal to

$$\sigma_{\text{RSS,statistical}} = \sqrt{\sigma_{x_{\text{Tx}}}^2 + \sigma_{y_{\text{Tx}}}^2 + \sigma_{z_{\text{Tx}}}^2} \approx \frac{2r\sigma_\rho}{d} \tag{15}$$

if $d_i = d$, $\sigma_{\rho_i} = \sigma_\rho$, $r_i = r$, and $\sigma_\rho \ll d$. In case of m uncorrelated measurements, σ_{RSS} is reduced by the factor $m^{-1/2}$, leading to $\sigma_{\text{RSS,statistical}} \approx (r\sigma_\rho)/(11d)$ for $m = 500$. Thus, for elliptical formation geometries, Eq. (15) can be used in the initial design phase of a relative navigation system as discussed here to obtain a rough estimate of the achievable 3-D RSS relative position accuracy.

The results in Table 3 further show that for a pendulum formation there is no dependency in the estimation accuracy on the antenna baseline d. Thus, three Rx antennas provide no geometrical advantage over a single Rx antenna in case of a long measurement arc and significant out-of-plane motion. A minor advantage comes from the increased number of measurements per measurement epoch (three instead of one), leading to a factor $3^{1/2}$ improvement in the estimation accuracy.

2. *Observability Analysis*

The estimation results from Table 3 are explained by performing an observability analysis for $\Delta\boldsymbol{x}_0^0 = \mathbf{0}$, as shown in Fig. 4. In Figs. 4a and 4b it is shown that for both formation geometries, v_6 is directed mainly towards an out-of-plane state for all values of $z_{\max}/r_e$ considered. However, as $z_{\max}/r_e$ increases, the vector rotates such that other states become more and more prominent, and thus, the out-of-plane state becomes relatively more observable. Not shown here is that, for the range of $z_{\max}/r_e$ considered, the largest component in v_5 is also an out-of-plane state.

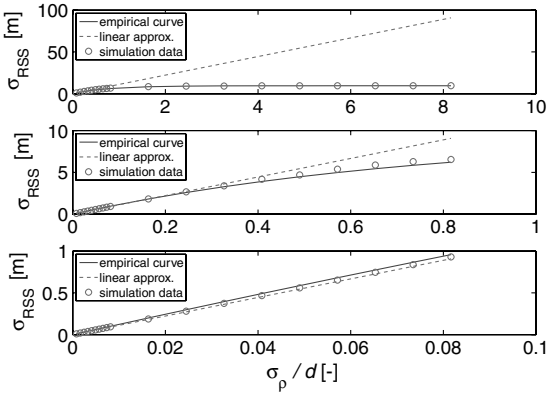

Fig. 3 RSS standard deviation in the relative position estimation for the safe ellipse for a measurement arc length of five orbits, $z_{\max} = r_e = 100$ m, and varying ranging accuracy. In the top, middle, and bottom plots, the antenna baseline is $(150)^{1/2}$ cm, $(150)^{1/2}$ dm, and $(150)^{1/2}$ m, respectively. Note the different scales for the axes.

In Figs. 4c and 4d, the magnitudes of λ_1, λ_2, λ_3, and λ_4 are shown to be independent on $z_{\max}/r_e$, whereas the magnitude of λ_5 and of λ_6 in Fig. 4d, is clearly dependent on $z_{\max}/r_e$. This results in a very poor conditioning of $\boldsymbol{G}$ for small $z_{\max}/r_e$, as two of the six eigenvalues have a very small value and, thus, will both have a large contribution in numerical errors when inverting the matrix $\mathbf{\Lambda} + \tilde{\boldsymbol{H}}^T\boldsymbol{W}\tilde{\boldsymbol{H}}$. Estimator divergence occurs for the safe ellipse when $\lambda_4/\lambda_5 > 10^2$ and occurs for the pendulum formation when $\lambda_4/\lambda_5 > 10^4$.

Figures 4c and 4d also show that λ_1 is much larger than the other eigenvalues. This indicates that the sensors are observing an unspecified state, which is equal to the linear combination of the states in eigenvector v_1 [23]. In Maessen and Gill [27], it is shown that this is indeed the case and that the most observable direction of the system, $(0.89, 0.01, 0.00, 0.01, 0.45, 0.00)^T$, is in fact the relative semimajor axis, which is equal to $4x + 2\dot{y}/n$ [20].

Figure 4c also shows that λ_6 is not dependent on $z_{\max}$ and is orders of magnitude smaller than the other eigenvalues, except for very small values for $z_{\max}/r_e$. Because of this, the most prominent states in eigenvector v_6 are always estimated with the worst accuracy, and the estimator result for the safe ellipse does not depend on $z_{\max}$.

Figure 5a shows that for the elliptical formation geometry and $\Delta\boldsymbol{x}_0^0 = \mathbf{0}$, an order of magnitude increase in d leads to an order of magnitude decrease in κ for all measurement arc lengths, which is caused by a two orders of magnitude increase of λ_6. For the elliptical formation geometry, the case with a single Rx antenna is not observable for $\Delta\boldsymbol{x}_0^0 = \mathbf{0}$ due to a very small value for λ_6 and is therefore not shown.

For the pendulum formation, a large antenna baseline positively influences the estimation result only for short measurement arcs of less than one orbit, see Fig. 5b. The factor $3^{1/2}$ difference in relative navigation accuracy between one and three Rx antennas for the pendulum formation, as shown in Table 3, is not apparent from Fig. 5b because this factor affects all eigenvalues and does, therefore, not affect κ. Comparing Figs. 5b and 5d shows that the shape of the plot in Fig. 5b depends on the magnitude of $z_{\max}$, whereas the magnitude of κ depends on r_e. Figure 5d also clearly demonstrates

Table 3 Estimation accuracies for a measurement arc length of five orbits

Formation	Out-of-plane distance	Single Rx antenna	Three Rx antennas
Safe ellipse	$z_{\max} = r_e$	$\sigma_{\text{RSS}} \approx 0.95\sigma^{\text{apr}}$	$\sigma_{\text{RSS}} \approx 0.95\sigma^{\text{apr}}(1 - e^{-1.3\sigma_\rho/d})$
	$z_{\max} \leq 0.1r_e$	Estimator divergence possible	Estimator divergence possible
Pendulum	$0.01r_e \leq z_{\max} \leq r_e$	$\sigma_{\text{RSS}} \approx \frac{3}{\sqrt{500}}\frac{r_e\sigma_\rho}{z_{\max}}$	$\sigma_{\text{RSS}} \approx \frac{3}{\sqrt{3}\sqrt{500}}\frac{r_e\sigma_\rho}{z_{\max}}$
	$z_{\max} < 0.01r_e$	Estimator divergence possible	Estimator divergence possible

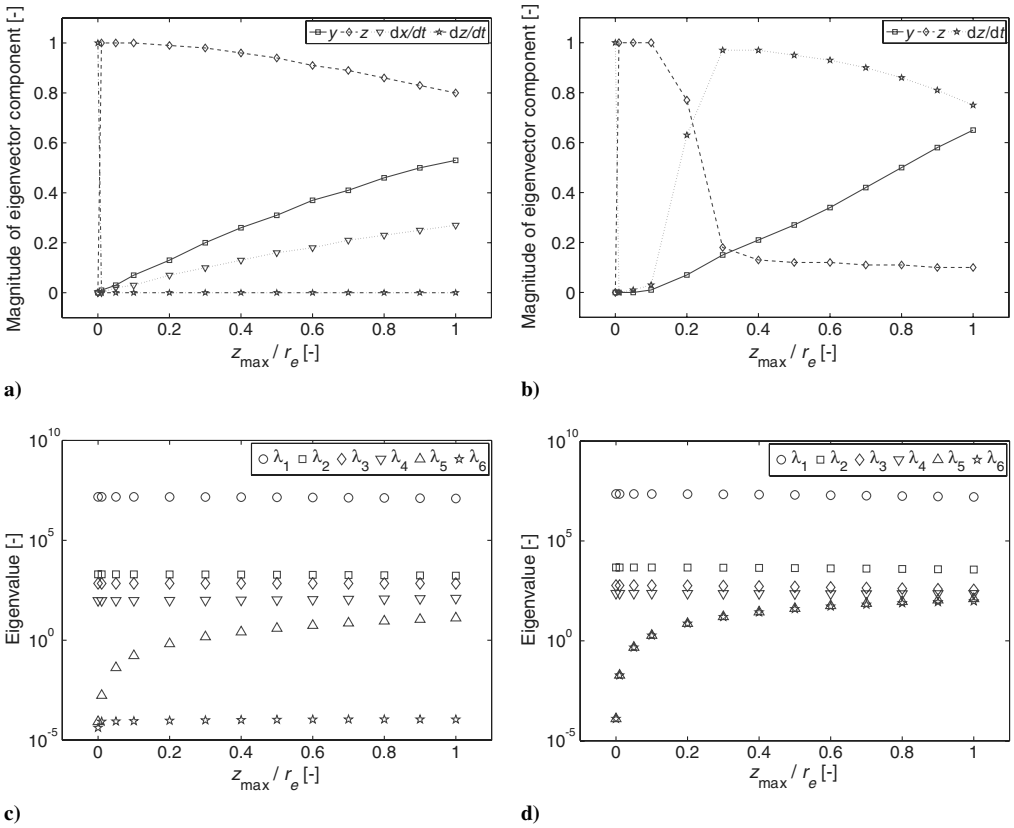

Fig. 4 Change in the direction of v_6 for Δx_0^0 in case of a) a safe ellipse and b) a pendulum formation and change in the magnitude of the eigenvalues of the Gramian for Δx_0^0 in case of c) a safe ellipse and d) a pendulum formation as a function of $z_{\max}/r_e$ for a measurement arc length of five orbits, $r_e = 1$ km, and $d = 150^{1/2}$ dm. In a) and b), the absolute value of the most significant eigenvector components is shown.

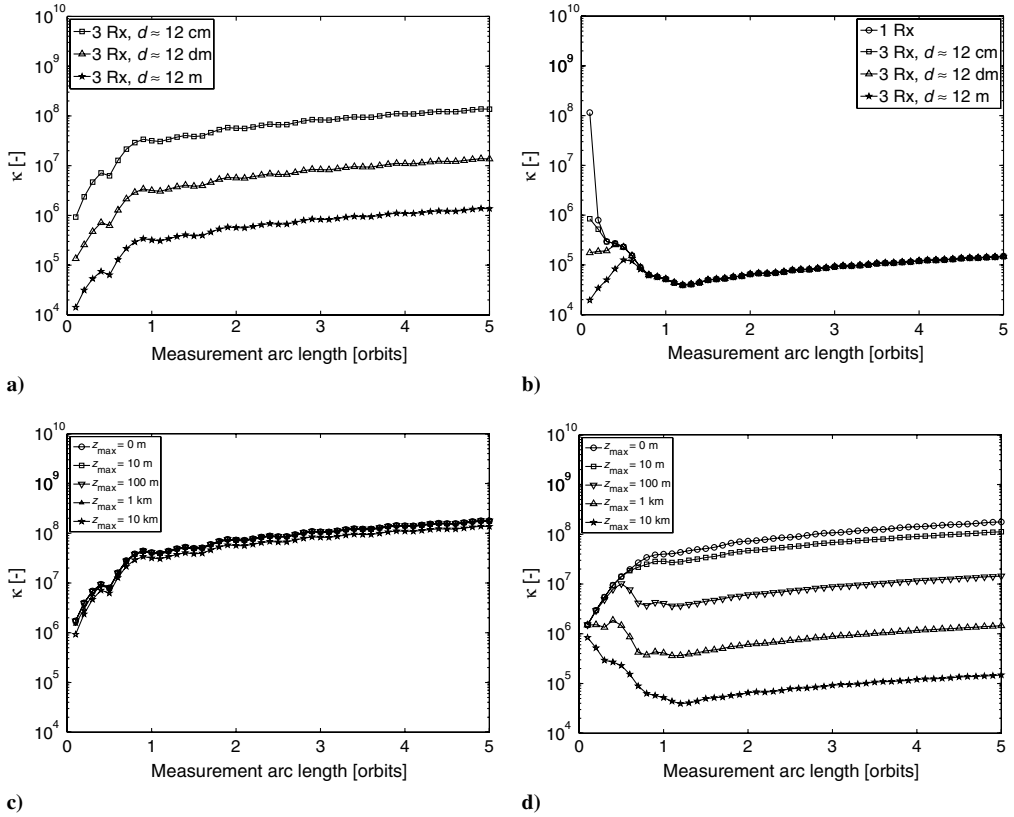

Fig. 5 Condition numbers for $\Delta x_0^0 = 0$ in case of a) an elliptical formation and b) a pendulum formation with $z_{\max} = r_e = 100$ m and different antenna baselines and in case of c) an elliptical formation and d) a pendulum formation with $r_e = 10$ km, $d = 150^{1/2}$ m, and different values for $z_{\max}$.

that for the pendulum formation a larger out-of-plane motion leads to improved observability, whereas Fig. 5c shows that this is hardly the case for the safe ellipse, which is consistent with earlier results.

VI. Conclusions and Future Work

An analytic derivation of the mean and the variance in the estimation of the position of a static transmitting antenna in a reference frame defined by three receiver antennas was performed. Analytical expressions were derived for the root sum squared standard deviation in the relative position estimation for elliptical and pendulum formations. For the elliptical formations, these results could be linked to the results from the statistical analysis. For the pendulum, this link is weaker due to the dependency of the result on the amount of relative out-of-plane motion. For both formation geometries, it was found that small out-of-plane motions lead to a high probability of estimator divergence. The probability of estimator divergence depends on the formation size, the antenna baseline, and the magnitude of the out-of-plane motion.

A detailed observability analysis was used to track down the root cause of the estimator divergence. It was found that the divergence is linked to the existence of a substantial gap between the two smallest eigenvalues of the system and the fourth largest eigenvalue of the system, leading to a bad conditioning of the Gramian matrix. The observability analysis also showed that the direction of the least observable direction of the system is a function of the amount of out-of-plane motion, but this direction is always mainly towards either the out-of-plane position or the out-of-plane velocity state.

In case of an elliptical formation geometry, a single receiver antenna does not provide sufficient information to make the system observable. For a pendulum formation with reasonable out-of-plane motion, however, a single Rx antenna does provide sufficient information to make the system observable and provides performance comparable to a system with three Rx antennas for measurement arc lengths of more than one orbit. For shorter measurement arc lengths, it is outperformed by systems using three Rx antennas. In general, for systems with three Rx antennas, the ratio of ranging accuracy versus antenna baseline should be as large as possible to provide the highest navigation accuracy.

Future work will focus on strategies that can improve the observability of the system, such as (temporarily) increasing the (relative) magnitude of the relative out-of-plane motion, performing an attitude maneuver, usage of different sensors, usage of a dynamic model that includes second-order effects, addition of one or more satellites in the relative state estimation, and a change of basis (e.g., using relative orbital elements).

References

[1] Markley, F., "Autonomous Navigation Using Landmark and Inter-Satellite Data," *AIAA/AAS Astrodynamics Conference*, AIAA, Seattle, WA, 20–22 Aug. 1984.

[2] Herklotz, R. L., "Incorporation of Cross-Link Range Measurements in the Orbit Determination Process to Increase Satellite Constellation Autonomy," Ph.D. Dissertation, Department of Aeronautics and Astronautics, Massachusetts Institute of Technology, Cambridge, MA, Dec. 1987, URI: http://hdl.handle.net/1721.1/14692.

[3] Psiaki, M., "Autonomous Orbit Determination for Two Spacecraft from Relative Position Measurements," *Journal of Guidance, Control, and Dynamics*, Vol. 22, No. 2, 1999, pp. 305–312. doi:10.2514/2.4379

[4] Liu, Y.-C., and Liu, L., "Orbit Determination Using Satellite-to-Satellite Tracking Data," *Chinese Journal of Astronomy and Astrophysics*, Vol. 1, No. 3, 2001, pp. 281–286. doi:10.1088/1009-9271/1/3/281

[5] Yim, J., Crassidis, J., and Junkins, J., "Autonomous Orbit Determination of Two Spacecraft System Using Relative Line of Sight Vector Measurements," *AAS/AIAA Spaceflight Mechanics Meeting*, AIAA, Maui, HI, 8–12 Feb. 2004.

[6] Woffinden, D., and Geller, D., "Relative Angles-Only Navigation and Pose Estimation for Autonomous Orbital Rendezvous," *Journal of Guidance, Control, and Dynamics*, Vol. 30, No. 5, 2007, pp. 1455–1469. doi:10.2514/1.28216

[7] Woffinden, D., and Geller, D., "Observability Criteria for Angles-Only Navigation," *IEEE Transactions on Aerospace and Electronic Systems*, Vol. 45, No. 3, 2009, pp. 1194–1208. doi:10.1109/TAES.2009.5259193

[8] Woffinden, D., and Geller, D., "Optimal Orbital Rendezvous Maneuvering for Angles-Only Navigation," *Journal of Guidance, Control, and Dynamics*, Vol. 32, No. 4, 2009, pp. 1382–1387. doi:10.2514/1.45006

[9] Chen, T., and Xu, S., "Double Line-of-Sight Measuring Relative Navigation for Spacecraft Autonomous Rendezvous," *Acta Astronautica*, Vol. 67, Nos. 1–2, July–Aug. 2010, pp. 122–134. doi:10.1016/j.actaastro.2009.12.010

[10] Doolittle, C., Chavez, F., and Lovell, T., "Relative Orbit Element Estimation for Satellite Navigation," *AIAA Guidance, Navigation, and Control Conference and Exhibit*, AIAA, San Francisco, CA, 15–18 Aug. 2005.

[11] Chavez, F. R., and Lovell, T. A., "Relative-Orbit Element Estimation for Satellite Navigation and Guidance," *AIAA/AAS Astrodynamics Specialist Conference and Exhibit*, AIAA,Providence, RI, 16–19 Aug. 2004.

[12] Holt, G., and Lightsey, E. G., "Sensor Considerations for Deep Space Formation Flying," *NASA/GSFC Spaceflight Mechanics Symposium*, NASA, Greenbelt, MD, 18–20 Oct. 2005.

[13] Kang, W., Ross, M., Pham, K., and Gong, Q., "Autonomous Observability of Networked Multisatellite Systems," *Journal of Guidance, Control, and Dynamics*, Vol. 32, No. 3, 2009, pp. 869–877. doi:10.2514/1.38826

[14] Matko, D., Rodič, T., Peljhan, M., Oštir, K., Dovžan, D., Mušič, G., Klančar, G., and Blažič, S., "The Design of Observers for Formation Flying Control," *6th International Workshop on Satellite Constellation and Formation Flying*, International Aeronautics Federation, Taipei, Taiwan, 1–3 Nov. 2010.

[15] Holt, G. N., and Lightsey, E. G., "In Situ Navigation of Spacecraft Formations in High-Altitude and Extraterrestrial Orbits," *Journal of Spacecraft and Rockets*, Vol. 45, No. 2, 2008, pp. 299–308. doi:10.2514/1.29361

[16] Huxel, P., "Navigation Algorithms and Observability Analysis for Formation Flying Missions," Ph.D. Dissertation, University of Texas at Austin, Austin, TX, 2006.

[17] Huxel, P. J., and Bishop, R. H., "Navigation Algorithms for Formation Flying Missions," *2nd International Symposium on Formation Flying Missions and Technologies*, NASA, Washington, D. C., 14–16 Sept. 2004.

[18] Huxel, P. J., and Bishop, R. H., "Navigation Algorithms and Observability Analysis for Formation Flying Missions," *Journal of Guidance, Control, and Dynamics*, Vol. 32, No. 4, 2009, pp. 1218–1231. doi:10.2514/1.41288

[19] Hill, G. W., "Researches in the Lunar Theory," *American Journal of Mathematics*, Vol. 1, No. 1, 1878, pp. 5–26. doi:10.2307/2369430

[20] Alfriend, K. T., Vadali, S. R., Gurfil, P., How, J. P., and Breger, L. S., *Spacecraft Formation Flying—Dynamics, Control and Navigation*, 1st ed., Elsevier Astrodynamics Series, Butterworth-Heinemann, Kidlington, UK, 2010, Chap. 5.

[21] Harr, J., Delpech, M., Grelier, T., Seguela, D., and Persson, S., "The FFIORD Experiment—CNES' RF Metrology Validation and Formation Flying Demonstration on PRISMA," *3rd International Symposium on Formation Flying Missions and Technologies*, European Space Agency, Noordwijk, The Netherlands, 23–25 April 2008.

[22] Dullerud, G. E., and Paganini, F., *A Course in Robust Control Theory: a Convex Approach*, Texts in Applied Mathematics, Vol. 36, Springer–Verlag, New York, 2000, Chap. 4.

[23] Ham, F. M., and Brown, R. G., "Observability, Eigenvalues, and Kalman Filtering," *IEEE Transactions on Aerospace and Electronic Systems*, Vol. AES-19, No. 2, 1983, pp. 269–273. doi:10.1109/TAES.1983.309446

[24] Kailath, T., Sayed, A. H., and Hassibi, B., *Linear Estimation*, Prentice-Hall, Upper Saddle River, NJ, 2000, Appendix A.4.

[25] Maessen, D. C., and Gill, E., "Relative State Estimation and Observability for Formation Flying Satellites in the Presence of Sensor Noise," *6th International Workshop on Satellite Constellation and Formation Flying*, International Astronautical Federation, Taipei, Taiwan, 1–3 Nov. 2010.

[26] Gelb, A., *Applied Optimal Estimation*, MIT Press, Cambridge, MA, 1974, Chap. 8.

[27] Maessen, D., and Gill, E., "Relative Orbital Element Estimation and Observability Analysis for Formation Flying Satellites using Inter-Satellite Range Measurements Only," *AIAA Guidance, Navigation, and Control Conference*, AIAA, Toronto, CA, 2–5 Aug. 2010.